JOURNAL OF THERMOPHYSICS AND HEAT TRANSFER
Vol. 13, No. 2, April–June 1999

Three-Dimensional Monte Carlo Simulations of Plume Impingement

Keith C. Kannenberg* and Iain D. Boyd†
Cornell University, Ithaca, New York 14853-7501

Three-dimensional plume impingement flows are simulated using the direct simulation Monte Carlo (DSMC) technique. Two impingement problems are computed. The impact of a jet of nitrogen on an inclined flat plate is considered. Good agreement is found between surface quantities calculated by DSMC and experimental data. A free molecular model of the plume is shown to provide reasonable estimates of impingement quantities. The plume of a hydrazine control thruster firing in a model satellite configuration is simulated. Surface quantities and net impingement effects are calculated. Free molecular analysis provides less accurate modeling of a multispecies flow with boundary-layer effects.

Nomenclature

A_P = plume constant
C = boundary-layer plume constant
C_P = specific heat at constant pressure
p = impingement pressure
q = heat flux
R_E = nozzle exit radius
r^* = throat radius
T_W = surface temperature
T_0, p_0 = stagnation temperature, pressure
U, ρ = plume velocity, density
α = local angle of incidence
γ = ratio of specific heats
δ_E = boundary-layer thickness at exit
η_t = net parallel efficiency
θ_{lim} = maximum inviscid turning angle
θ_0 = boundary-layer streamline angle
ρ^* = throat density
σ = accommodation coefficient
τ = shear stress

Introduction

SPACECRAFT in orbit require propulsion systems for various functions such as attitude control and stationkeeping. Low-thrust rockets are often employed to meet these requirements. The gas plume that is produced during a thruster firing may impinge on spacecraft surfaces. Impingement can have a number of undesirable effects such as the production of additional forces and torques, heat loads, and surface contamination. Each of these effects can reduce the overall lifespan of the spacecraft. Accurate modeling of plume impingement is an important factor in spacecraft design.

Numerical simulations of thruster plumes can be used to characterize and predict impingement effects. At the extremely low densities seen in a plume expanding into vacuum, continuum fluid mechanics becomes invalid. The direct simulation Monte Carlo (DSMC) method simulates the gas at the microscopic level and can capture nonequilibrium effects occurring in a rarefied plume flow. DSMC has been successfully applied to nonequilibrium flows in propulsion, hypersonics, and materials processing,[1–4] as well as to plume impingement flows.[5,6]

The goal of this work is to validate the capability to simulate complex plume impingement flows using the DSMC technique. To demonstrate this capability, two different three-dimensional impingement flows are examined. The first flow considered is the impingement of a jet on an inclined flat plate. Experimental measurements of impingement quantities are used to verify the numerical results. The second flow is the impingement of a hydrazine thruster plume on a solar array in a model satellite configuration. Free molecular theory is used to model both flows analytically.

Numerical Method

The simulations presented in this study are performed using a three-dimensional version of MONACO, a numerically efficient implementation of the DSMC method.[7] MONACO is a general-purpose DSMC code designed for workstation architectures. It is designed to be applicable to a wide range of flow problems without requiring problem-specific modifications. It can be run on a single machine or in parallel on an arbitrary number of processors.

Free Molecular Analysis

In the far field of a low-density plume expansion, the flow reaches very low densities and large Knudsen numbers. Under these highly rarefied conditions, the plume can be reasonably approximated as being collisionless. With this assumption, impingement quantities on a surface located within the plume can be calculated analytically. This free molecular analysis provides a limiting case for surface quantities.

Under the assumption of free molecular flow, surface quantities are a function only of the incoming freestream particles. Particles scattering off of the surface do not have any further interaction with the surface or the incoming gas. The net mass, momentum, and energy transferred to the surface is obtained by integrating over the incoming and outgoing particle distribution functions.[8]

If the incoming gas is assumed to have an equilibrium velocity distribution at the hypersonic limit, the pressure is given by

$$p = \tfrac{1}{2}\rho U^2\{2(2-\sigma)(\sin\alpha)^2 + \sigma\sqrt{\pi[(\gamma-1)/\gamma]}\sqrt{(T_w/T_0)}\sin\alpha\} \quad (1)$$

Similar expressions are obtained for shear stress, heat transfer, and flux.

Presented as Paper 98-2755 at the AIAA/ASME 7th Joint Thermophysics and Heat Transfer Conference, Albuquerque, NM, June 15–18, 1998.

*Graduate Student, Mechanical and Aerospace Engineering Department. Student Member AIAA.

†Associate Professor, Mechanical and Aerospace Engineering Department. Member AIAA.

In the hypersonic limit, the fluid velocity is further approximated by the limiting result from isentropic theory, $U_{\lim} = \sqrt{2C_pT_0}$.

The density of the gas is modeled using the plume model of Simons.[9] This model describes the density as a function of the throat density and location in the plume expressed in polar coordinates measured from the center of the exit plane. The plume density is given by

$$\rho(r, \theta)/\rho^* = A_P(r^*/r)^2 f(\theta) \tag{2}$$

$$f(\theta) = \{\cos[(\pi/2)(\theta/\theta_{\lim})]\}^{2/(\gamma-1)}, \qquad \theta \le \theta_0$$
$$= f(\theta = \theta_0)e^{-C(\theta-\theta_0)}, \qquad \theta_0 < \theta < \theta_{\lim} \tag{3}$$

where θ_0 is the angle between the plume axis and the streamline separating the boundary layer from the isentropic core, and $\theta_{\lim}$ is the maximum turning angle of a streamline at the exit for inviscid flow. The constant C is given by

$$C = \tfrac{3}{2}A_P\sqrt{(\gamma+1)/(\gamma-1)}(R_E/2\delta_E)^{(\gamma-1)/(\gamma+1)} \tag{4}$$

These parameters are calculated analytically as a function of the stagnation conditions, gas properties, and source geometry.[10]

The relations for plume density and velocity can be used with expressions for surface quantities such as Eq. (1) to obtain expressions for impingement quantities in terms of distance from the orifice, location in the plume, and the angle of incidence:

$$p = p_0 A_P f(\theta)\left(\frac{r^*}{r}\right)^2\left(\frac{2}{\gamma+1}\right)^{1/(\gamma-1)}\left(\frac{\gamma}{\gamma-1}\right)$$
$$\times\left[2(2-\sigma)(\sin\alpha)^2 + \sigma\sqrt{\pi\frac{\gamma-1}{\gamma}\frac{T_w}{T_0}}\sin\alpha\right] \tag{5}$$

$$\tau = 2\sigma p_0 A_P f(\theta)\left(\frac{r^*}{r}\right)^2\left(\frac{2}{\gamma+1}\right)^{1/(\gamma-1)}\left(\frac{\gamma}{\gamma-1}\right)\cos\alpha\sin\alpha$$

$$q'' = \sigma\sqrt{2RT_0}p_0 A_P f(\theta)\left(\frac{r^*}{r}\right)^2\left(\frac{2}{\gamma+1}\right)^{1/(\gamma-1)} \tag{6}$$
$$\times\sqrt{\frac{\gamma}{\gamma-1}}\left[\frac{\gamma}{\gamma-1} - \frac{\gamma+1}{2(\gamma-1)}\frac{T_w}{T_0}\right]\sin\alpha$$

$$F = nU$$
$$= \frac{p_0}{m}A_P f(\theta)\left(\frac{r^*}{r}\right)^2\left(\frac{2}{\gamma+1}\right)^{1/(\gamma-1)}\sqrt{\frac{2}{RT_0}\frac{\gamma}{\gamma-1}} \tag{7}$$

Inclined Flat Plate

Impingement of a jet onto an inclined flat plate represents one of the simplest possible three-dimensional impingement problems. The relatively simple geometry allows it to be readily investigated both numerically and experimentally while still retaining three-dimensional effects.

The problem under consideration is a freejet impacting on a flat plate. A plume of molecular nitrogen is generated by a sonic orifice. The orientation of the plate is varied relative to the axis of the plume. Figure 1 shows a schematic of the configuration.

This study considers one particular set of orifice inlet conditions—unheated flow ($T_0 = T_W = 300$ K) expanding from a stagnation pressure of 1000 Pa. The orifice itself is circular in cross section and 1 mm in radius, and the flow is assumed to be sonic at the exit. The Knudsen number based on orifice radius is 8×10^{-3} at the orifice exit. These conditions ensure a rarefied plume flow suitable for calculation using the DSMC method. The impingement surface is located a distance of 40 mm from the orifice measured perpendicular to the surface (distance L in Fig. 1). The flow conditions and geometry yield a plume constant $A_P = 0.617$ and a turning angle $\theta_{\lim} = 130.5$ deg.

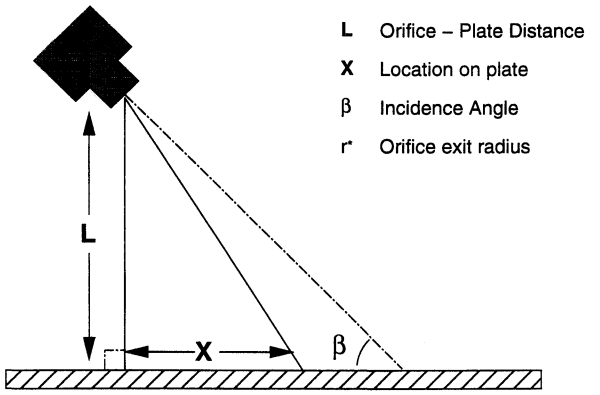

Fig. 1 Schematic of flat-plate impingement.

Experimental Study

The plate impingement configuration was investigated experimentally at DLR, German Aerospace Research Center, Germany. Measurements of impingement pressure and shear stress were taken by Legge,[11] and measurements of heat flux were made by Döring.[12] A variety of stagnation pressures, plate orientations, and separations were considered.

Pressure and shear stress data were obtained using a pressure balance that directly measured the force on a floating element. Heat flux data were obtained by measuring the rate of change of surface temperature using thermocouples. Data were taken on the surface along a line that is coplanar with the plume axis.

The experiments were performed in the high vacuum facility in Göttingen, Germany. The background pressure of the facility was 0.045 Pa during pressure and shear measurements with the stagnation pressure considered in the present study (1000 Pa). The background pressure was twice this value (0.090 Pa) during the heat transfer experiment.

Pressure and shear-stress data were normalized to eliminate the effect of stagnation pressure and plate separation L. The following normalizations were used:

$$\hat{p} = (p/p_0)(L/r^*)^2 \tag{8}$$

$$\hat{\tau} = (\tau/p_0)(L/r^*)^2 \tag{9}$$

While this normalization does reduce the data to a significant degree, some dependence on the stagnation pressure is still observed. A reduction in stagnation pressure results in an increase in normalized pressure and shear stress as a result of the increasing rarefaction of the plume. For the present study, data obtained using a stagnation pressure of 1000 Pa are used whenever possible.

Physical Modeling

The inlet flow at the sonic orifice is modeled as a macroscopically uniform stream of molecular nitrogen directed along the axis of the plume. The effects of a boundary layer at the exit are assumed to be small and are neglected. Inlet properties are calculated from isentropic theory assuming sonic conditions at the exit and stagnation conditions of 1000 Pa and 300 K. This corresponds to a velocity of 323 m/s, a temperature of 252.2 K, and a number density of 1.53×10^{23} m^{-3}. A background gas pressure is imposed to simulate the effects of the experimental tank pressure.

The impingement surface is modeled assuming diffuse reflection with full accommodation to a constant surface tem-

perature (σ = 1.0). The surface temperature is equal to the stagnation temperature of the plume (300 K).

Computational Modeling

Fully unstructured grids using tetrahedral cells are used. Grids are generated using an advancing front package called FELISA. Cell sizes are approximately scaled to the local mean free path. Figure 2 shows an example of a grid for the case with the plume axis parallel to the surface (β = 0 deg). Only the boundary mesh is shown. The majority of cells are in the vicinity of the nozzle where the density is highest. Compression at the surface is relatively small because of the low densities involved. As a result, the surface grid at the plate (not shown) consists of approximately uniform triangles for the cases considered. Symmetry planes are employed to reduce the size of the domain. Two planes are used in the normal impingement (β = 90 deg) case, and one each in the other cases.

The simulation time step is varied across the domain, with each cell using a unique value. The local time step is scaled by the cell size that is approximately proportional to the inverse of the local density.

Simulations are load balanced for parallel execution using a simple scheme that groups cells according to the Z coordinate of their geometric center. The number of cells assigned to each processor is chosen to distribute particles evenly among processors.

Typical parameters for the three-dimensional plume simulations are summarized next. Computational cost parameters for plate impingement: grid cells = 300,000; number of particles = 3.5 million; transient steps = 22,500; sampling steps = 5,000; calculation time = 14 h; and steady state η_t = 95%. The calculations are performed using 16 nodes of an IBM SP-2.

Comparison of Surface Quantities

Impingement quantities are examined for several orientations of the plate. Comparison with experimental data is used to verify the accuracy of the DSMC simulations of the plume and impingement. Comparison with predictions from the free molecular model provides an estimate of the accuracy of this theory for simple impingement flows as well as a qualitative basis for comparison with the simulation at the far ends of the surface where experimental data are not available.

In the case of normal impingement of the plume (β = 90 deg), the experimental data are taken along a radial line extending out from the axis. The simulation data set includes data across the entire surface presented as a function of distance from the axis. In the other cases, both the experimental and simulation data sets are taken along a line on the surface that is coplanar with the plume axis.

Normal Impingement (β = 90 Deg)

Figure 3 compares normalized surface pressures for simulation, experiment, and free molecular theory. Good agreement is found between the data sets. The profiles show the same general shape: pressure falling from a maximum at the axis. The DSMC and theoretical profiles show an asymptote at the background pressure at large distances from the axis, where the plume has a minimal effect on the surface.

The simulation underpredicts the experimental values by a significant amount (as much as 60%) at the far extent of the experimental data set. The smooth asymptotic shape seen in the DSMC and theoretical profiles is not as apparent in the measurements far from the axis. The slower decrease in pressure with distance from the axis may indicate difficulties in measuring pressures at the low densities away from the axis. It may also indicate a higher tank pressure in the facility than is reported.

Normalized shear stress is considered in Fig. 4. Good agreement is observed between the simulation, experiment, and theory. The profiles each show the same shape with stress rising from zero at the plume axis to a maximum and then falling with decreasing gas pressure. DSMC stresses exceed the free molecular values far from the axis. This is likely a result of particles that strike the surface, undergo collisions with the incoming plume, and are scattered back to the surface at a high angle of attack.

Surface heat flux is shown in Fig. 5. The simulation captures the trend of the experimental measurements and predicts the magnitude of the heat flux away from the axis. The simulation does overpredict the heat flux considerably near the axis (X/L < 0.75).

Significant fluctuations appear in the numerical heat-flux results, with the magnitude of the fluctuations increasing with distance from the axis. This is primarily a result of the sample size of particles striking the surface. The total number of particles sampled per cell is on the order of 10^4 near the axis and

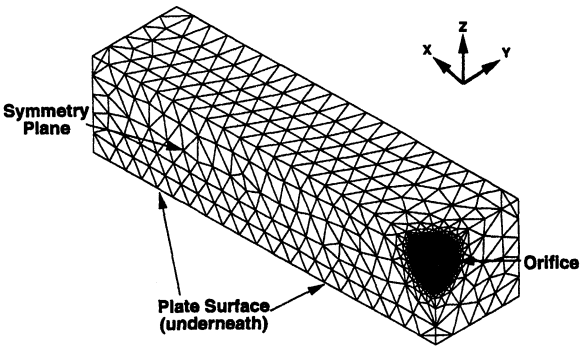

Fig. 2 Surface grid for β = 0-deg case.

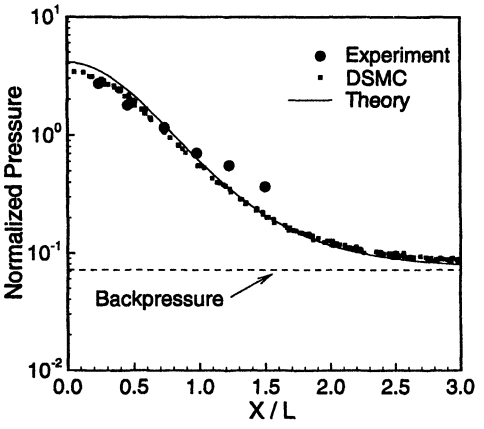

Fig. 3 Comparison between DSMC and measured surface pressures at β = 90 deg.

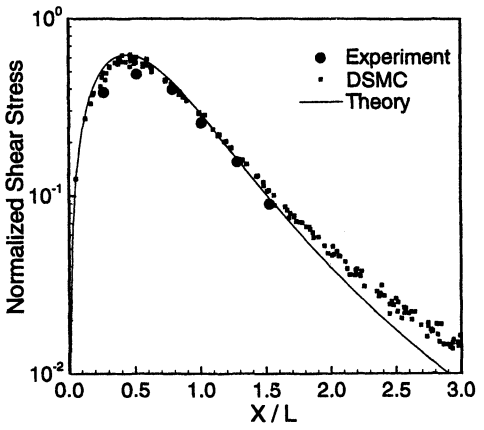

Fig. 4 Surface shear stress for β = 90 deg. Comparison between DSMC, experiment, and free molecular theory.

decreases with radial distance, up to a factor of 3 at the farthest radial extent. The statistical fluctuations in the DSMC simulation are magnified in the calculation of energy transfer that involves the second moment of the particle velocities.

The theoretical curve has the same shape as the DSMC result, but shows a larger magnitude of heat transfer. The difference increases as the axis is approached. Gas densities are larger near the axis, and consequently, the mean free path and Knudsen number are smaller. The assumption of free molecular flow is weakest near the axis and collisional effects are more significant. This tends to lower the energy transfer below the free molecular value. The deviation is greater in terms of heat transfer than in pressure or shear stress because energy is a second moment of the particle distribution function.

β = 45-Deg Case

Figure 6 shows surface pressure profiles for the β = 45-deg case. Good agreement is again found between the simulation and experimental data sets as well as free molecular theory. The point of maximum pressure is just downstream of the point directly below the orifice, where the effects of density and angle of attack are high. The pressure drops off asymptotically to the background value to both sides of this maximum; this is more rapid behind the orifice.

The experimental data are again higher than the DSMC and theoretical values at both ends of the profile. The magnitude of the pressures at these points are comparable to that seen at the end of the β = 90-deg profile. This points toward uncertainty in pressure measurements at low densities or a higher back pressure in the facility.

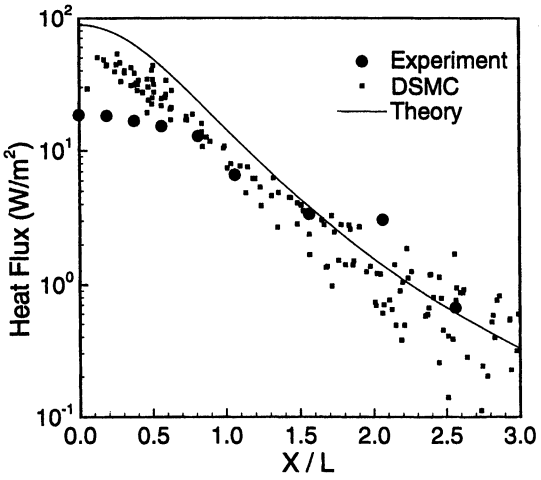

Fig. 5 Surface heat flux for β = 90 deg. Comparison between DSMC, experiment, and free molecular theory.

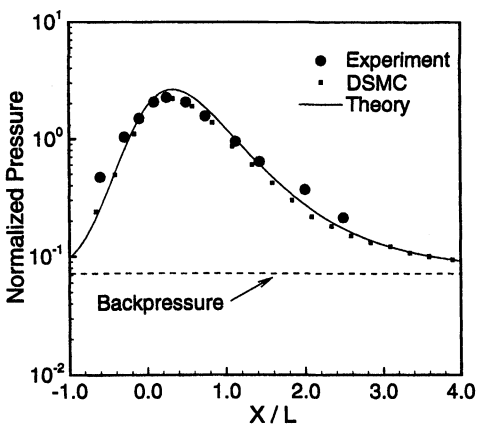

Fig. 6 Surface pressure for β = 45 deg. Comparison between DSMC, experiment, and free molecular theory.

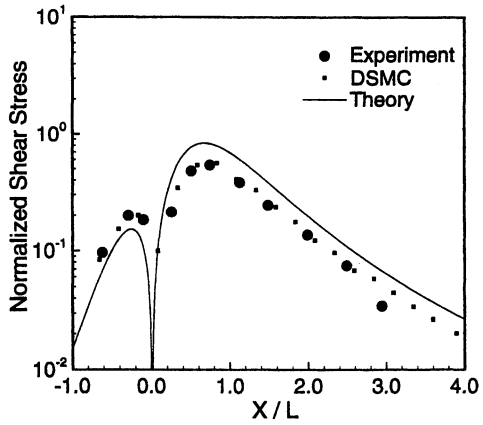

Fig. 7 Surface shear stress for β = 45 deg. Comparison between DSMC, experiment, and free molecular theory.

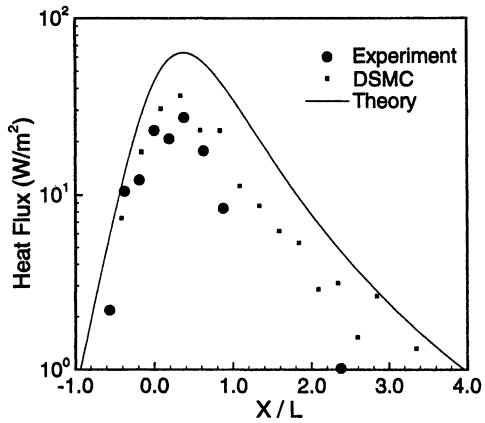

Fig. 8 Surface heat flux for β = 45 deg. Comparison between DSMC, experiment, and free molecular theory.

Shear-stress profiles are reported in Fig. 7. The DSMC stresses show excellent agreement with the experimental data. The features of the experimental profile are captured by the simulation, particularly the rapid decrease that occurs directly below the orifice.

While the qualitative structure of the free molecular profile agrees with those of the simulation and experiment, the theoretical profile differs in terms of magnitude. In front of the orifice ($X/L > 0$), the free molecular stresses overpredict the simulation and measured values. Behind the orifice ($X/L < 0$), the free molecular stresses underpredict the actual stresses. This is likely a result of the presence of backscattered particles that strike the surface behind the orifice.

Heat transfer profiles are reported in Fig. 8. Although significant fluctuations are again seen in the simulation and experimental results, there is generally good agreement between the data sets. Free molecular theory overpredicts heat transfer across most of the range considered because of collisional effects. This effect is countered to some extent behind the orifice by backscattered particles that tend to increase the transport of energy to the surface.

Parallel Impingement (β = 0 Deg)

Before presenting comparisons with experimental data, it is important to note that the DLR study by Legge[11] does not report pressure or shear-stress data for the parallel impingement case with a stagnation pressure of 1000 Pa. The lowest stagnation pressure for which β = 0-deg pressure and shear data are reported is 4000 Pa. The study by Döring[12] does present heat flux data for a stagnation pressure of 1000 Pa. The DSMC simulations use a stagnation pressure of 1000 Pa. Although the data are normalized by the stagnation pressure,

Legge reports some effect of flow rarefaction on the normalized surface quantities, particularly shear stress.

The difference in stagnation pressures complicates the modeling of tank pressure effects. The ratio of background to stagnation pressure is not a constant in the experimental facility, generally falling with increasing stagnation pressure. Consequently, the parallel impingement case has been simulated without backpressure and the theoretical pressure profile is for expansion into a vacuum.

Surface pressures for the parallel impingement case are shown in Fig. 9. The profiles show good qualitative agreement. Without a backpressure, the simulation and theoretical profiles drop toward zero at the ends of the plate. No asymptote is seen

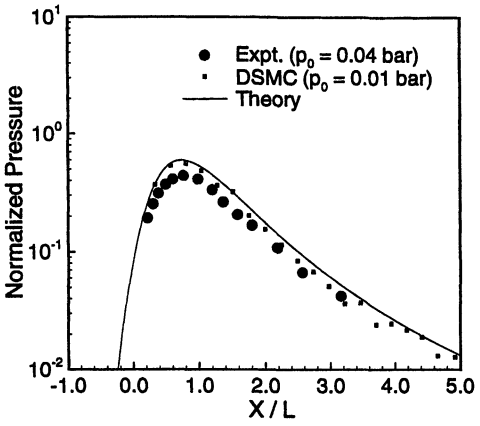

Fig. 9 Surface pressure for β = 0 deg. Comparison between DSMC, experiment, and free molecular theory.

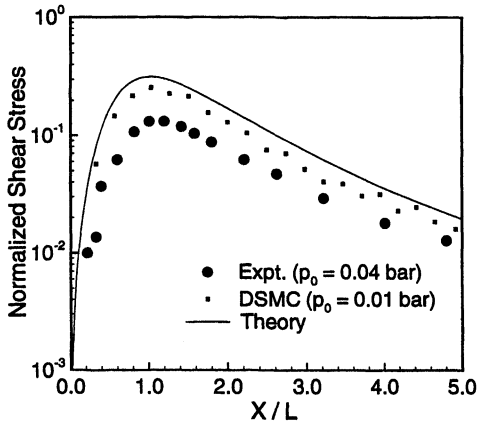

Fig. 10 Surface shear stress for β = 0 deg. Comparison between DSMC, experiment, and free molecular theory.

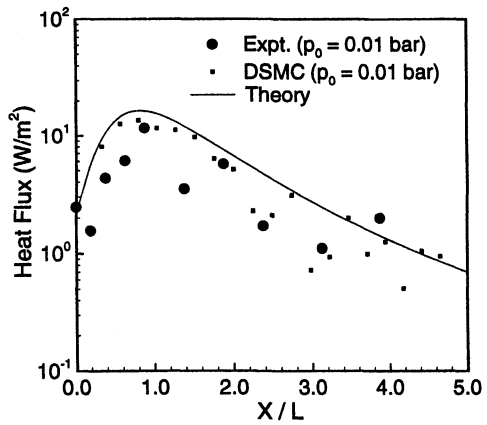

Fig. 11 Surface heat flux for β = 0 deg. Comparison between DSMC, experiment, and free molecular theory.

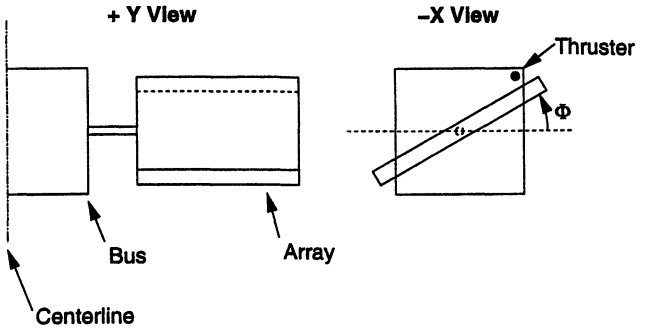

Fig. 12 Schematic of model satellite configuration.

in the experimental data because the normalized facility pressure (not shown) is significantly lower with the higher stagnation pressure. The lower experimental pressures are a result of a higher stagnation pressure and lower Knudsen number at the surface.

Shear stress data are shown in Fig. 10. The profiles again show qualitative agreement. The experimental values are lower because of higher densities. The effect on shear is stronger than that on pressure. This was previously reported by Legge.[11] The effect of rarefaction can be seen to a much smaller degree in a comparison between simulation and free molecular results. The DSMC values are slightly lower because of collisional effects.

Heat transfer results are presented in Fig. 11. Experimental heat-flux data are based on a stagnation pressure of 1000 Pa, equal to that used in the DSMC simulation. At the low densities involved in the parallel impingement case, statistical fluctuations are quite large in both the experimental and numerical results. The simulation results overpredict the data to some degree, although the trend is captured quite well. The free molecular results do not significantly overpredict the heat transfer as was seen in the other cases. This is likely a result of the low densities found at the surface for this case.

Model Satellite Configuration

A representative satellite geometry consisting of a spacecraft bus and solar arrays is simulated as a model impingement configuration. A plume is generated by a hydrazine control thruster mounted at the corner of one side of the spacecraft bus. Fig. 12 shows a schematic of the problem. The spacecraft bus is a 1.5-m cube of which half is simulated. The array section is 3.25 m long, 2.5 m wide, and 0.12 m thick, and is deployed 0.75 m from the spacecraft. Expansion of the plume and its impingement on the solar array panel are modeled. Two orientations of the array with respect to the bus are considered.

The thruster is modeled after an operating hydrazine control thruster, the MR-103-series 0.2-lbf REA, manufactured by Primex Aerospace Company. This thruster was originally developed for the Voyager 1 and 2 spacecraft and is also in use on such programs as GPS, Iridium, Cassini, and various communications satellites. This study will consider an operating mode at 60% of the rated thrust. Relevant data for the thruster‡ are shown next: Operating conditions and parameters for hydrazine thruster: nominal thrust = 0.55 N, expansion ratio = 100:1, half angle = 15 deg, exit radius = 2.921 mm, chamber pressure = 1.25 MPa, stagnation temperature = 1167 K, and flow rate = 2.62×10^{-4} kg/s.

Physical Modeling

The gas plume is a three-species mixture of molecular nitrogen, hydrogen, and ammonia. Simulations begin at the exit plane of thruster using flow properties based on a numerical calculation of flow in the thruster. Exit plane number densities

‡Morris, J., private communication, Primex Aerospace Co., Redman, WA, 1997.

taken from this earlier calculation are scaled down by a factor of 1.52 to maintain consistency with the experimentally measured mass flow of the device. At the centerline the inlet flow has the following properties: 2200 m/s velocity, 500 K temperature, and 3.2×10^{23} m^{-3} total density.

Because of the relatively low temperature of the plume, it can be considered chemically frozen. Vibrational energy modes are likewise frozen. All spacecraft surfaces are modeled as diffuse reflectors with full accommodation. Surfaces are maintained at 273 K. Surface chemistry and adsorption are not considered in these calculations.

Computational Modeling

Simulations are performed in two parts. First, an axisymmetric calculation of the near-field plume in the vicinity of the thruster is performed. Data from this calculation are then used as input for the three-dimensional calculation of the plume far field and impingement. Separation of the calculation in this manner greatly reduces the cost of the overall calculation.

Near Field

The near field expansion of the plume is considered to be an axisymmetric problem that is independent of the surrounding geometry. The flow domain is hemispherical and extends more than 10 exit radii out from the center of the thruster exit. The grid is an unstructured mesh with cell sizes and time steps scaled according to the local mean free path.

Inflow conditions for the far-field calculation are taken at the breakdown surface. This is the locus of points for which the breakdown parameter[13] equals the threshold value $P = 0.02$. To more readily use this as a geometric interface between the near- and far-field simulations, the surface is simplified to a capped cylinder with uniform cross section. Density in the near field is shown in Fig. 13 along with the location of the interface surface.

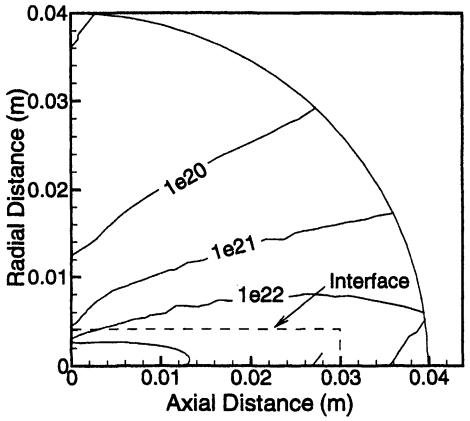

Fig. 13 Contours of number density for the axisymmetric near-field simulation. The interface surface is indicated.

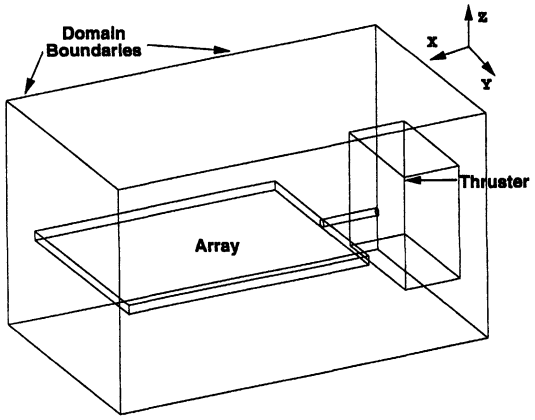

Fig. 14 Boundaries of the computational domain. Shown for unrotated array case, Φ = 0 deg.

Far Field and Impingement

The far-field simulation considers the whole area surrounding the spacecraft, including the solar array. The computational domain is an orthogonal parallelepiped that extends beyond the spacecraft surface by at least 0.25 m in each coordinate direction. Only one-half of the spacecraft is simulated. The boundaries of the computational domain are shown in Fig. 14. The solar array is shown in the nominal, unrotated configuration (Φ = 0 deg).

An unstructured mesh consisting of tetrahedral cells is employed. The mesh is generated using the grid-generation package FELISA. Cell sizes are approximately scaled according to local density. Variable time steps are employed with cell size being used as a scaling factor.

To improve resolution in the vicinity of the interface surface where flow density is highest, a simple scheme of particle weight scaling is employed. Cells in the immediate vicinity of the inflow (interface) surface are assigned a low particle weight, 10% of the reference value for the simulation. The band of cells immediately outside this surface are assigned a weight of 40% of the reference value. The remaining cells are assigned the reference weight. Figure 15 shows this weight scheme on a plane cut taken along the axis of the cylindrical inflow surface. This scaling roughly follows the density variation in close proximity to the inflow. Because there is only a small number of particles moving toward the inflow in this highly supersonic flow, there is a minimal amount of cloning involved. The weight scheme allows reasonable resolution of the high-density region without affecting the accuracy of the calculation.

The computational parameters for the near- and far-field plume calculations are summarized in Table 1.

Results

Impingement simulations were performed for two orientations of the solar array, Φ = 0 deg and Φ = +30 deg. Of

Table 1 Computational cost parameters for model satellite configuration

Parameter	Near field	Far field
Grid size	7600 cells	290,000 cells
Number of particles	425,000	2,900,000
Transient steps	12,500	18,000
Sampling steps	10,000	10,000
Calculation time	5 h	11 h
Number of processors	4	16
Parallel efficiency	97%	91%

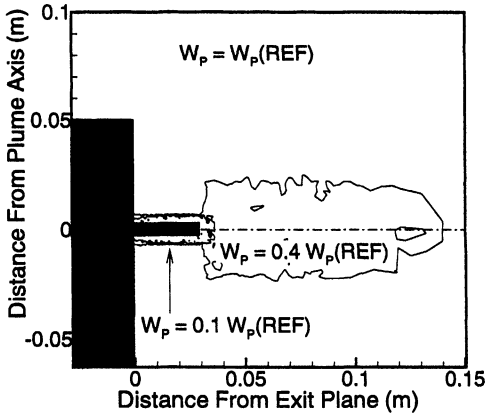

Fig. 15 Particle weight scaling in the vicinity of the inflow surface.

primary importance are the mass, momentum, and energy imparted to the array by the plume. Figures 16 and 17 show distributions of surface pressure for the 0- and +30-deg cases. The view is in the plane of the array. The contour plots show maximum values at the near end of the array toward the $+Y$ side, closest to the thruster. In the Φ = 0-deg case, the maximum pressure is downstream of the leading edge as a result of the influence of the nozzle boundary layer. As expected, impingement pressures are larger in the Φ = +30-deg case, where the array is tilted toward the thruster.

Ammonia molecules are the major contamination concern with hydrazine thrusters. Figures 18 and 19 show distributions of ammonia flux on the array. The qualitative behavior of this property is very similar to that observed with pressure.

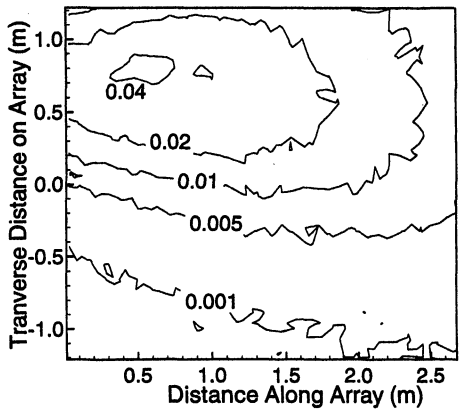

Fig. 16 Contours of impingement pressure (Pa) at the array surface for the 0-deg array case.

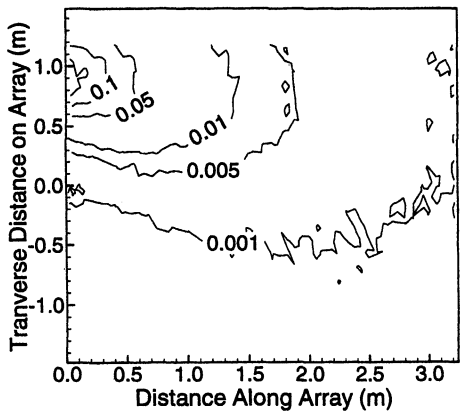

Fig. 17 Contours of impingement pressure (Pa) at the array surface for the 30-deg array case.

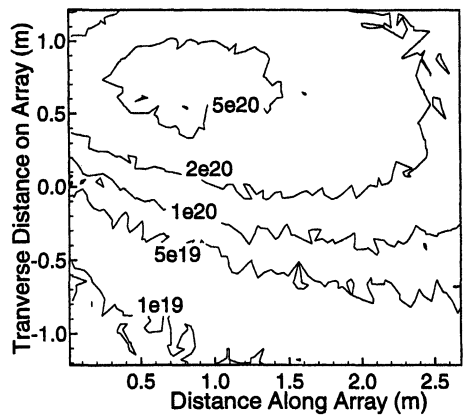

Fig. 18 Contours of NH_3 flux (no./m^2 s) at the array surface for the 0-deg array case.

Data extracted along a line on the array surface are used to quantitatively examine the surface quantities. Data are taken on the line that intersects the array top surface and the plane parallel to the array axis that contains the plume axis.

The operating conditions for the hydrazine thruster can be used to calculate the plume parameters A_P, θ_{lim}, θ_0, and C. There is some uncertainty involved in this calculation when a multispecies gas is considered. To be most useful from an engineering standpoint, the free molecular results should be based on stagnation conditions and the geometry of the nozzle. The expressions for surface quantities [Eqs. (5–7)] depend on gas properties R and γ, which are difficult to determine a priori for a rarefied gas in which individual species will have varying mole fractions and velocities. In this study, the gas has been

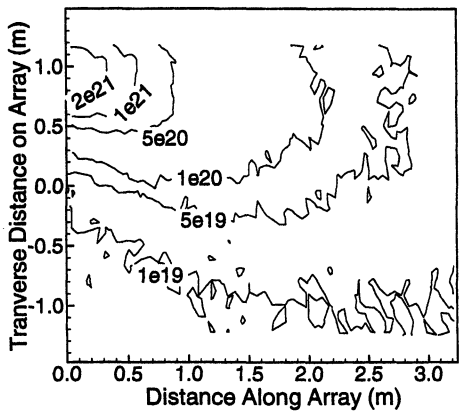

Fig. 19 Contours of NH_3 flux (no./m^2 s) at the array surface for the 30-deg array case.

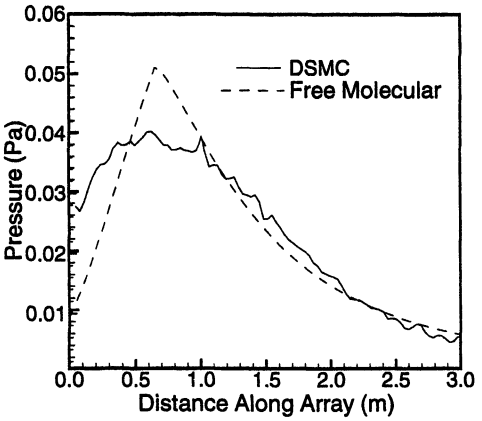

Fig. 20 Comparison of simulation and free molecular pressures on array surface for 0-deg array case.

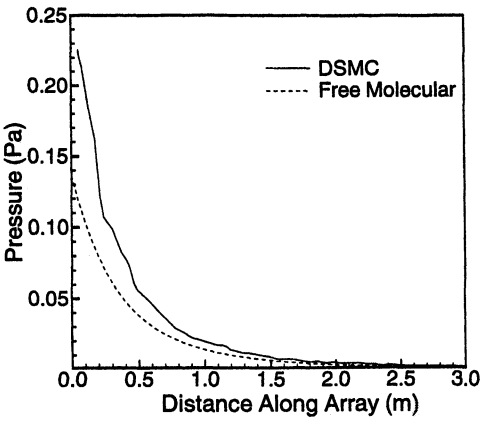

Fig. 21 Comparison of simulation and free molecular pressures on array surface for 30-deg array case.

assumed to have a constant molecular weight and ratio of specific heats using values reported for the exit plane (M = 13 kg/mol, γ = 1.4). These parameters yield a plume constant, A_P = 3.62, boundary-layer constant, C = 12.6, and limiting angle, θ_0 = 19.2 deg and θ_{lim} = 58.7 deg.

Figure 20 shows impingement pressure profiles for the 0-deg case. Reasonable agreement is found on the far end of the array, but at the near end the free molecular result falls well below the simulation. The noticeable drop in the free molecular profile on the upstream side of the array is a result of boundary-layer effects. The drop in pressure can be seen in the simulation as well, but it is not as dramatic. The sharp decline indicates that the density model falls too rapidly in the boundary-layer regime.

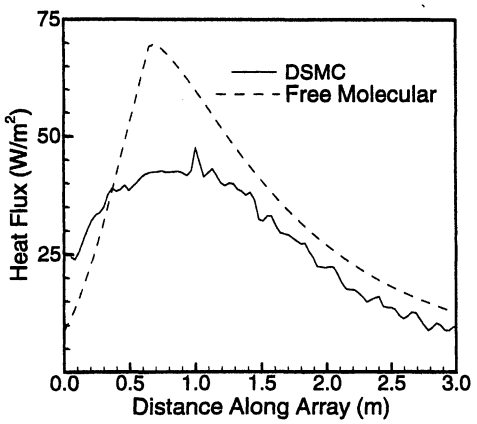

Fig. 22 Comparison of simulation and free molecular heat flux on array surface for 0-deg array case.

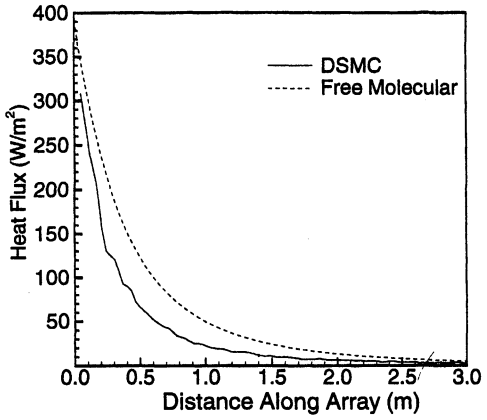

Fig. 23 Comparison of simulation and free molecular heat flux on array surface for 30-deg array case.

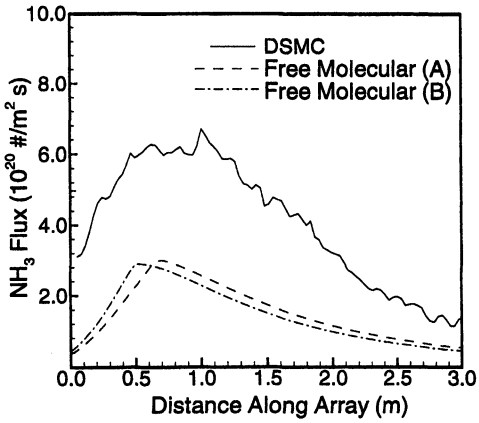

Fig. 24 Comparison of simulation and free molecular NH_3 flux on array surface for 0-deg array case.

The 30-deg case is shown in Fig. 21. In this case, the array is rotated toward the thruster, and as a result the profile being considered is significantly closer to the thruster. The linear profile is within the core of the plume, and consequently, there is no drop in pressure on the upstream side of the plate as a result of the boundary layer. Both the simulation and analytical profiles primarily show an inverse squared drop in pressure with distance, which is consistent with the density model. The DSMC results predict a 70% higher pressure across the length of the array. This may indicate a low estimate of the plume constant A_P.

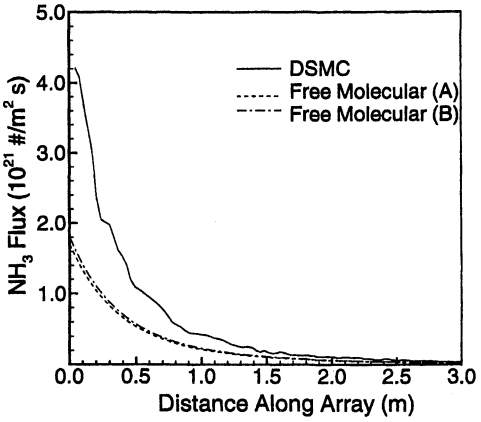

Fig. 25 Comparison of simulation and free molecular NH_3 flux on array surface for 30-deg array case.

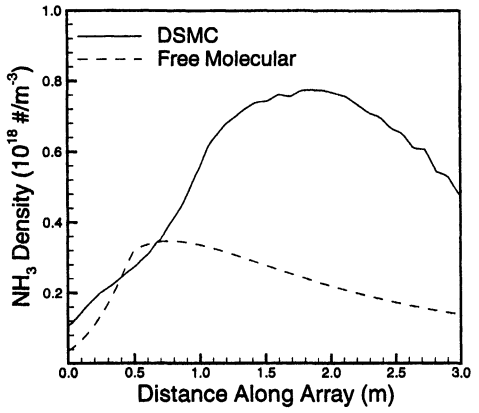

Fig. 26 Comparison of NH_3 densities from stand-alone plume simulation and free molecular model. Data at location of array surface for 0-deg case.

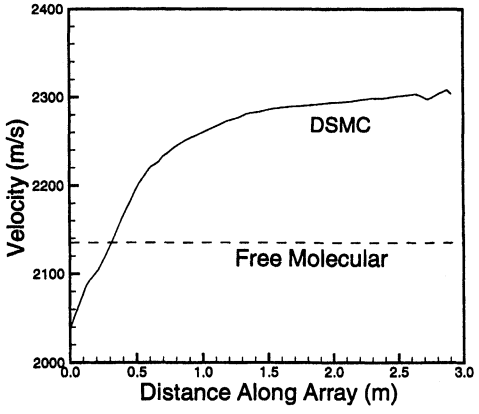

Fig. 27 Comparison of NH_3 velocities from stand-alone plume simulation and free molecular model. Data at location of array surface for 0-deg case.

Figures 22 and 23 show heat transfer profiles. In both cases the behavior is very similar to that of surface pressure. The free molecular profile for 0 deg shows an extreme drop on the upstream end while otherwise matching the shape of the DSMC profile. In the 30-deg case the DSMC and theoretical profiles are qualitatively similar. In both cases the free molecular values tend to exceed the simulation heat transfer. Overprediction of heat flux is consistent with the results for flat-plate impingement.

The number density flux of ammonia striking the array is shown in Figs. 24 and 25. Two free molecular profiles are shown for each case. The first (labeled A) assumes a constant species composition in the plume model and a uniform limiting velocity based on the average molecular weight. The second (B) calculates the ammonia flux as if the plume was composed entirely of ammonia with the correct number density. The two methods produce essentially the same fluxes.

Qualitatively, the flux profiles show the same behavior for both pressure and heat transfer. Both angle cases show significantly higher DSMC fluxes. This indicates the difficulty of applying the free molecular model to a multispecies, rarefied gas.

The problems with the free molecular model for flux are illustrated by a simulation of the thruster plume flowfield without any impingement surfaces. This plume flow should give a reasonable estimate of what the impingement surfaces see, because the boundary layer caused by the impingement is small. Figure 26 plots ammonia density for the freely expanding plume at the same spatial location as the linear profiles shown for the 0-deg case in Fig. 24. The DSMC results are compared with density predicted by the Simons plume model (assuming an ammonia plume, method B discussed earlier).

Figure 27 compares simulated ammonia velocities and the limiting velocity employed in the free molecular analysis ($\sqrt{2C_pT_0}$). Downstream of where the leading edge of the solar array would be located, within the isentropic core of the plume, DSMC densities are on average two times higher than the Simons model predicts. DSMC velocities are also 5–8% larger than the analytical model. Because the number density flux in free molecular flow is the product of density and velocity [Eq. (7)], these factors combine to produce the significantly larger fluxes seen in the DSMC results shown in Fig. 24.

In the boundary-layer region, the relationship between plume properties and impingement flux is less clear. However, near the upstream edge, the simulation again produces significantly higher ammonia densities, which again would lead to larger flux. The more complex density profile seen in the DSMC result, likely caused by differing mole fractions and velocity slip between the species, again indicates the limitations of the analytical plume model for complex gas flows.

The total forces and torques imparted to the array are important for spacecraft design. The total amount of a contaminant such as ammonia striking the surface is also important. Tables 2 and 3 summarize these integrated quantities for the two simulations. Integrated quantities calculated from free molecular theory are also included.

It is worthy to note that in both cases the net force exerted on the array by the plume is on the order of 20% of the nominal 0.55 N thrust of the thruster. This interaction force is primarily in the $+X$ direction, which is opposite to the thrust vector and thus acts to reduce the effective thrust of the device. As a result, nearly 20% of the propulsion energy is wasted.

Little net difference is seen between the two array orientations. Although part of the array is closer to the thruster in the 30-deg case, the average angle of attack over the array is higher, which reduces the impingement quantities. The rotation causes a portion of the array to be significantly farther from the thruster, reducing the effective area over which force is exerted.

Comparison between the simulation and free molecular values follows the same pattern shown in the linear profiles. The net forces are comparable, which is consistent with similar pressures. Free molecular flow predicts a higher energy transfer and a significantly lower net flux of ammonia, both consistent with the previous comparisons.

In all of the previous analyses and simulations, surfaces were assumed to be fully accommodating. A more accurate representation of a real surface would assume partial accommodation. An accommodation coefficient σ of 0.8 is typical for a metallic surface. Table 4 compares integrated impingement effects for full and partial accommodation. As expected, net heat transfer to the array scales with accommodation coefficient. The net force in the x direction, parallel to the plume axis, is a result of surface shear, and consequently, also scales with σ. The other two force components and torque are essentially unaffected by a change in accommodation coefficient. These quantities are primarily caused by surface pressure that scales nonlinearly with σ.

Examination of the comparisons in Table 4 and the expression for impingement pressure [Eq. (5)] indicate that the surface model will have some effect on the net impingement effects. Heat transfer will be overpredicted by a fully diffuse model. Momentum transfer will be overpredicted if it is primarily a result of shear forces. If more direct impingement is involved, such as might occur in a docking maneuver, the effect is less clear and will depend on the surface and plume temperatures and the geometry through angle of attack. These

Table 2 Integrated impingement effects for Φ = 0 deg

Impingement property	DSMC	Free molecular
Net force, X component, N	0.100	0.118
Net force, Y component, N	−0.0107	−0.00588
Net force, Z component, N	−0.0814	−0.0647
Net centerline torque, Nm	0.0405	0.0369
Net heat transfer, W	101	112
Net incidence of NH_3, s^{-1}	1.44×10^{21}	470×10^{20}

Table 3 Integrated impingement effects for Φ = +30 deg

Impingement property	DSMC	Free molecular
Net force, X component, N	0.0922	0.148
Net force, Y component, N	0.0228	0.0226
Net force, Z component, N	−0.0645	−0.0563
Net centerline torque, Nm	0.0519	0.0509
Net heat transfer, W	88.3	137
Net incidence of NH_3, s^{-1}	1.43×10^{21}	6.15×10^{20}

Table 4 Effect of accommodation coefficient on free molecular integrated impingement effects

Impingement property	Φ = 0 deg, σ = 1.0	Φ = 0 deg, σ = 0.8	Φ = +30 deg, σ = 1.0	Φ = +30 deg, σ = 0.8
Net force, X component, N	0.118	0.0945	0.148	0.118
Net force, Y component, N	−0.00588	−0.00471	0.0226	0.0227
Net force, Z component, N	−0.0647	−0.0656	−0.0563	−0.0531
Net centerline torque, Nm	0.0369	0.0377	0.0509	0.0490
Net heat transfer, W	112	89.5	137	109

observations should hold for both an analytical model and DSMC simulations.

Conclusions

The DSMC method provides reasonably accurate modeling of impingement flows. Generally good agreement with experimental data for the plate problem indicates that the plume and impingement effects are modeled correctly, although there is some tendency to overpredict surface heat flux. The calculation of a satellite configuration demonstrates the ability to simulate real engineering configurations. Calculations are expensive in three dimensions, but can be performed efficiently in parallel. Careful use of variable scaling can reduce the overall cost significantly.

Free molecular theory provides a reasonable estimate of surface quantities at high Knudsen numbers. The analysis tends to overpredict the values, however, with heat transfer and shear stress being more sensitive to the degree of rarefaction than pressure. Boundary-layer and multispecies effects are not properly handled by the simple plume model.

Problems that can be broken down into two distinct parts such as the near and far field of a plume can be more efficiently computed using two separate simulations. If the first portion can be computed assuming axial symmetry, the overall cost can be reduced significantly. This type of hybrid approach is particularly appropriate for engineering problems, where simulations of a number of far-field problems may be begun using a single near-field result.

Acknowledgments

The authors gratefully acknowledge the financial support of John H. Glenn Research Center at Lewis Field through Grant NAG3-1451 and the U.S. Air Force Office of Scientific Research under Grant F49620-96-1-0210. Computational resources were provided by the Cornell Theory Center and the National Aerodynamic Simulation program at NASA Ames Research Center.

References

[1]Boyd, I. D., and Stark, J. P. W., "Modeling of a Small Hydrazine Thruster Plume in the Transition Flow Regime," *Journal of Propulsion and Power*, Vol. 6, No. 2, 1990, pp. 121–126.

[2]Boyd, I. D., Penko, P. F., Meissner, D. L., and DeWitt, K. J., "Experimental and Numerical Investigations of Low-Density Nozzle and Plume Flows of Nitrogen," *AIAA Journal*, Vol. 30, No. 10, 1992, pp. 2453–2461.

[3]Boyd, I. D., Candler, G. V., and Levin, D. A., "Dissociation Modeling in Low Density Flows of Air," *Physics of Fluids*, Vol. 7, No. 7, 1995, pp. 1757–1763.

[4]Font, G. I., and Boyd, I. D., "Numerical Study of the Effects of Reactor Geometry on a Chlorine Helicon Etch Reactor," *Journal of Vacuum Science and Technology A*, Vol. 15, No. 2, 1997, pp. 313–319.

[5]Ivanov, M. S., Markelov, G. N., Kashkovsky, A. V., and Giordano, D., "Numerical Analysis of Thruster Plume Interaction Problems," *Proceedings of the 2nd European Spacecraft Propulsion Conference*, European Space Agency, SP-398, 1997, pp. 603–610.

[6]Lumpkin, F. E., Stuart, P. C., and Le Beau, G. J., "Enhanced Analyses of Plume Impingement During Shuttle-Mix Docking Using a Combined CRD and DSMC Methodology," AIAA Paper 96-1877, June 1996.

[7]Dietrich, S., and Boyd, I. D., "Scalar and Parallel Optimized Implementation of the Direct Simulation Monte Carlo Method," *Journal of Computational Physics*, Vol. 126, 1996, pp. 328–342.

[8]Schaaf, S. A., and Chambré, P. L., *Flow of Rarefied Gases*, Princeton Univ. Press, Princeton, NJ, 1961.

[9]Simons, G. A., "Effect of Nozzle Boundary Layers on Rocket Exhaust Plumes," *AIAA Journal*, Vol. 10, No. 11, 1972, pp. 1534, 1535.

[10]Legge, H., and Boettcher, R. D., "Modelling Control Thruster Plume Flow and Impingement," *Rarefied Gas Dynamics*, Plenum, New York, 1985, pp. 983–992.

[11]Legge, H., "Plume Impingement Forces on Inclined Flat Plates," *Rarefied Gas Dynamics*, VCH Press, Weinheim, Germany, 1991, pp. 955–962.

[12]Döring, S., "Experimental Plume Impingement Heat Transfer on Inclined Flat Plates," DLR, German Aerospace Research Center, TR IB 222-90 A 36, Germany, Sept. 1990.

[13]Bird, G. A., *Molecular Gas Dynamics*, Clarendon, Oxford, England, UK, 1994.